ALBAII VACUUM SYSTEM: DESIGN EVOLUTION AND PROTOTYPING*

R. Parise†,[1], B. Francisco[1], L. Carvajal[1], J. Álvarez[1], O. Traver[1], G. Peña[1], L. Ribo[1], P. Salmerón[1], M. Llonch[1], M. Quispe[1], N. Gonzalez[1], J. Casas[1], F. Perez[1], K. Blümer[2], R. Schwertfeger[2], H. Henninger[2], C. Colldelram[1]
[1]ALBA Synchrotron, Cerdanyola del Vallès, Spain
[2]FMB Feinwerk- und Messtechnik, Berlin, Germany

Abstract

ALBA is upgrading its storage ring into a 4th-generation diffraction-limited facility, which demands redesigned vacuum chambers. Most of the 268.8 m ring, divided into 16 arcs, will use OFHC-Cu or CuCrZr to dissipate synchrotron radiation and minimize resistive-wall impedance. To meet the injection-efficiency requirements, former 16 mm circular cross-section has been replaced by a rhombic geometry providing a 22 mm horizontal aperture, 1.25 mm wall thickness and clearances of 1 mm to the magnet poles. Its structural response shows 13 MPa maximum stress with deformations of 3 µm. A short bellows is foreseen between each pair of BPM blocks to absorb chamber displacements from alignment tolerances and thermal expansions while keeping BPM positions fixed. At dipole positions, antechambers with crotch absorbers manage the radiation heat load, with each arc receiving 20.5 kW of power. The entire ring will be NEG-coated to accelerate conditioning and reach the required pressure of 1×10^{-9} mbar at 100 Ah. This contribution presents the vacuum system status and the design, fabrication progress of the prototypes.

INTRODUCTION

ALBA is upgrading its storage ring into ALBA II, a 4th-generation diffraction-limited synchrotron light source [1]. The compact lattice imposes strong constraints on the vacuum system, including magnet aperture, synchrotron radiation power, conductance, impedance, and injection-efficiency requirements. To satisfy these constraints, the chamber design has evolved from the previously planned 16 mm circular cross-section to a rhombic profile with increased horizontal aperture. This paper presents the vacuum concept, the chamber geometry optimization, and the status of the prototype fabrication program.

ALBAII VACUUM SYSTEM CONCEPT

The ALBA II vacuum system follows a modular arc concept combining compact integration, distributed NEG pumping, and synchrotron radiation power management. Each arc forms one vacuum section delimited by two gate valves, with NEG-coated chambers activated ex-situ before installation.

A typical arc includes five copper-alloy dipole chambers, five pumping locations, and five crotch absorbers, while part of the synchrotron radiation is distributed directly onto the chamber walls. Eleven BPMs are foreseen per arc: seven as standalone BPM/bellows assemblies and four integrated into dipole chambers. Short bellows are foreseen between BPM blocks to absorb alignment tolerances and thermal expansion while preserving the BPM positions.

The dipole chambers use OFS/OFHC copper or CuCrZr depending on thermal and mechanical requirements. They combine a rhombic beam aperture, integrated cooling, antechambers for synchrotron radiation extraction, pumping blocks, and crotch absorbers at selected locations. Compact MO-type flanges are used where space is critical, while adapted CF ones are kept where required.

DESIGN EVOLUTION

The initial vacuum chamber concept was based on a 16 mm circular internal cross-section. Further lattice and injection studies showed that this aperture was too restrictive to meet the required injection efficiency [2]. As a result, alternative chamber profiles were investigated to increase the horizontal aperture while preserving compatibility with the existing magnet geometry [3], as adopted in other compact storage rings [4,5]. A rhombic cross-section, similar to Elettra 2.0 [4], was selected as the most promising option.

Since the magnet poles were kept fixed, and a minimum clearance of 1 mm to the chamber wall had to be maintained, the available external envelope imposed a strong geometrical constraint. Figure 1 shows the resulting available area obtained from the superposition of the surrounding magnet pole profiles. The boundary corresponds to a 1 mm offset from the nearest magnet pole, and the previously 16 mm circular cross-section is shown for reference.

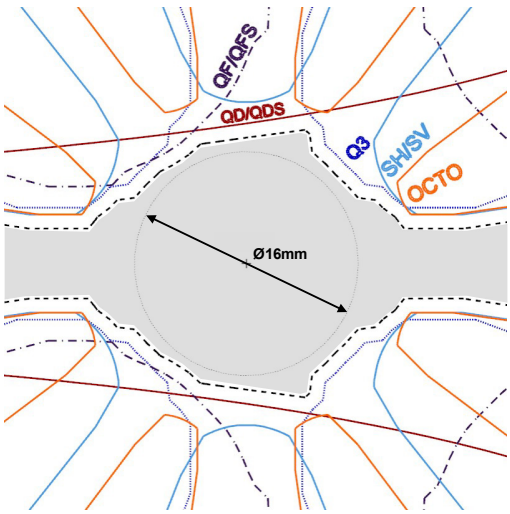

Figure 1: Available chamber envelope.

* Work supported by Spanish MCIN and the European Union – NextGenerationEU project 28.50.460D.74903 from the Recovery and Resilience Mechanism.
† rparise@cells.es

Within this constrained envelope, the chamber geometry was optimized to increase the horizontal aperture while limiting mechanical stress and deformation. Vacuum conductance, transverse beam impedance, and manufacturability were also considered, with the internal cross-sectional area maximized where possible and minimum radii constrained by available machining tools.

These objectives were converted into optimization targets: ensuring at least the minimum aperture required for injection, maximizing internal area and vertical aperture, minimizing stress and deformation, and identifying feasible wall thickness values. The parameter ranges are summarized in Table 1.

Table 1: Parameter Ranges Used in the Optimization

Parameter	Lower bound [mm]	Upper bound [mm]
Corner diameters	1.4	14
Wall thickness	0.8	1.5
Horizontal aperture	20	22

Rhombic chamber geometries were parameterized using wall thickness, horizontal aperture, vertical aperture, and the two internal corner diameters as the main variables. An elliptical profile was also analysed for comparison. The main geometrical parameters are shown in Fig. 2.

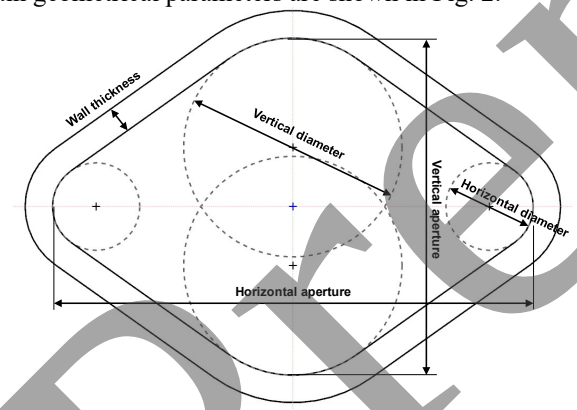

Figure 2: Geometry parameterization.

Structural analyses were performed in ANSYS using C10200 OFHC copper. The model used approximately 19,500 elements, with atmospheric pressure of 0.1 MPa applied to the chamber cross-section and weak springs for numerical stabilization. The design space was then explored using response-surface-based Adaptive Multiple-Objective Optimization, combining initial parameter sampling, surrogate model generation, and adaptive refinement of the optimization front. The resulting solutions provide candidate geometries with their corresponding stress, deformation, and parameter sensitivity. An example of the resulting equivalent-stress distribution for a rhombic chamber cross-section is shown in Fig. 3.

Beam impedance and vacuum conductance were also evaluated for the analysed geometries. Vacuum conductance was estimated under molecular-flow conditions and normalized to the previously planned 16 mm circular cross-section. For a fixed chamber length, the conductance scales approximately with A^2 / P, where A is the cross-sectional area and P the perimeter [6]. The relative conductance was therefore estimated as:

$$\frac{C_2}{C_1} = \frac{{A_2}^2}{{A_1}^2} \cdot \frac{P_1}{P_2}$$

where C_1 corresponds to the 16 mm circular reference and C_2 to the analysed geometry. To estimate the pressure impact, the gas load was assumed proportional to the internal wall area and therefore to the perimeter [6]. Since $p \propto Q/C$, the relative pressure scales as:

$$\frac{p_2}{p_1} = \frac{{A_1}^2}{{A_2}^2} \cdot \frac{{P_2}^2}{{P_1}^2}.$$

This estimate assumes the same specific outgassing rate and neglects variations in effective NEG pumping speed, which are expected to be secondary due to the large NEG-coated surface available. It should therefore be interpreted only as a first-order geometric comparison.

As a first-order transverse impedance indicator, the comparison used the minimum beam-to-wall distance. Assuming similar chamber families and neglecting changes in the geometry form factor, the transverse impedance scales approximately with the inverse cube of this distance, so:

$$\frac{Z_{\perp,2}}{Z_{\perp,1}} \approx \left(\frac{d_1}{d_2}\right)^3.$$

This estimate is used only as a comparative indicator, since the real impedance depends on the full chamber shape, material, coating, and frequency spectrum [7].

Manufacturability was evaluated mainly through wall thickness and minimum internal corner diameters. The lower wall-thickness limit was set to 0.8 mm, although thinner chambers have been reported in the literature [8]. Corner diameters were constrained by the available machining tools, with a minimum tool diameter of 2.5 mm, and by the need to avoid local collapse or excessive deformation under atmospheric pressure.

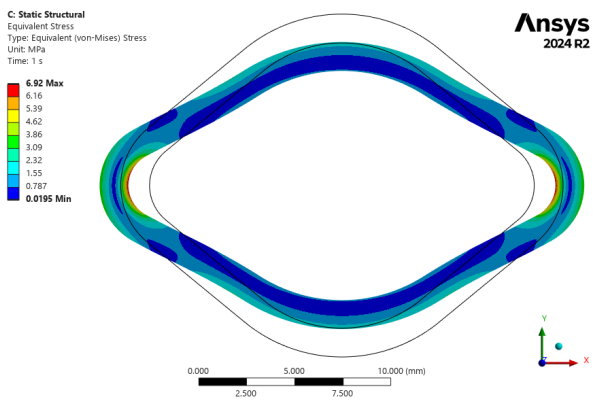

Figure 3: Example of equivalent-stress distribution under atmospheric pressure.

RESULTS AND DISCUSSION

After hundreds of cases, the optimization showed that wall thickness is the dominant parameter in the trade-off between mechanical robustness and vacuum performance. Within the fixed external envelope, increasing wall thickness reduces stress and deformation, but also reduces the internal area and the minimum beam-to-wall distance, penalizing conductance, the geometric pressure indicator, and the transverse impedance indicator.

The horizontal aperture is mainly driven by injection requirements: 20 mm is the minimum acceptable value, while 21 mm and 22 mm options were evaluated to provide additional margin for fabrication, assembly, and alignment tolerances. Under the fixed external envelope imposed by the magnet poles, increasing the horizontal aperture constrains the internal corner diameters, affecting the mechanical response. It also improves the shadowing of downstream components, since the conical absorber tip remains fixed with respect to the beam centre while the chamber wall moves outward, increasing the protected region at the chamber exit.

In summary, larger wall thickness improves the mechanical response at the expense of vacuum and impedance performance, while larger horizontal aperture improves injection margin but increases the geometric challenge under the fixed magnet envelope.

The elliptical profile was also evaluated but discarded, since the largest geometry fitting within the magnet-constrained envelope produced a largest inscribed circle of only 9.8 mm, well below the 13.1 mm limit associated with the transverse impedance criterion

Among the evaluated cases, the selected geometry provides the largest horizontal aperture considered while keeping stress, deformation, conductance loss, and the geometric pressure penalty within acceptable limits. The selected geometry has a wall thickness of 1.25 mm, a horizontal aperture of 22 mm, and a vertical aperture of 15.4 mm. The horizontal and vertical corner diameters are 4.0 mm and 10.0 mm, respectively. The largest circle that can be inscribed in the chamber cross-section has a diameter of 14.4 mm, corresponding to a minimum beam-to-wall distance of 7.2 mm. Compared with the previously planned 16 mm circular cross-section, this gives an estimated 37% increase in the transverse impedance indicator. The conductance is reduced by only 0.3%, while the geometric pressure indicator increases by about 10%. Structurally, the maximum stress is 13 MPa, below the 15 MPa design limit, and the maximum deformation is approximately 3 μm.

PROTOTYPING PROGRAM STATUS

The ALBA II vacuum prototyping program was launched to validate the manufacturability of the most critical components before series production [9]. The current focus is on the QD1 long dipole chamber in CuCrZr with an integrated absorber, the QDS1 short dipole chamber in OFHC-Cu with a dedicated absorber port, and a Glidcop® photon absorber. These prototypes address the main technical risks of compact geometry, synchrotron radiation power management, NEG-coating compatibility, and tight integration with the magnet lattice.

Fabrication has progressed, although several manufacturing issues have affected the schedule. The QDS1 photon absorber initially failed to achieve leak-tightness during brazing, most likely due to a raw material issue in the Glidcop®. After unsuccessful re-brazing attempts, the component was remanufactured. Additional brazing qualification tests using Glidcop® and AISI 316LN stainless steel samples from the same batch were successful, and the final brazed and welded assembly has been confirmed leak-tight. Dimensional verification, bake-out, and functional testing are ongoing.

The QD1 and QDS1 chambers were also affected by earlier manufacturing issues during key process steps. For the QDS1 chamber, a problem occurred during wire electrical discharge machining, while the QD1 chamber was affected by a critical electron beam welding issue. These issues led to delays and required additional process development before continuing with final fabrication.

The current status is more advanced. For QD1, all individual chamber bodies have been delivered and checked by CMM, and the single bodies are being prepared for electron beam welding after completion of additional welding tests. Electron beam welding trials of the key-hole contour were successful, while tests on the thin-wall tube remain under development. The following steps include EB welding of the chamber sections, leak testing, dimensional inspection, final machining, and the last EBW operation. For QDS1, all individual bodies have also been delivered and checked by CMM. The first chamber section has been brazed and successfully He-leak tested, while preparation of the second section for brazing is ongoing. The next operations include brazing of the second section, flange machining and welding, and the final brazing step of the complete chamber. If the remaining processes progress as planned, fabrication of both chambers before NEG coating is expected to be completed by mid-June.

Despite the delays, the prototypes remain essential for validating fabrication specifications and qualification procedures, particularly regarding copper-alloy machining, joining, cooling integration, leak-tightness, and NEG-coating preparation. These lessons remain directly applicable to the final chamber design despite the latest geometry update.

CONCLUSION

The ALBA II vacuum chamber design has evolved from the previously planned 16 mm circular profile to a rhombic cross-section driven by injection-efficiency requirements and constrained by the magnet aperture. The selected geometry provides a 22 mm horizontal aperture with acceptable mechanical response and moderate vacuum and impedance penalties. In parallel, the prototyping program continues to validate the key manufacturing routes, including copper-alloy machining, joining, cooling integration, leak-tightness, and NEG-coating preparation. These results will support the final chamber specifications and the transition toward series production.

REFERENCES

[1] F. Perez, "ALBA II Accelerator Upgrade Project Status", presented at IPAC'26, Deauville, France, May. 2026, paper THP2009, this conference.

[2] G, Benedetti *el al.*, "Status of lattice studies for ALBA-II", presented at IPAC'26, Deauville, France, May. 2026, paper WEP5034, this conference.

[3] J. Marcos *et al.*, "Status of magnets for ALBA II project: design, prototyping and production plans", presented at IPAC'26, Deauville, France, May. 2026, paper MOP7065, this conference.

[4] L. Novinec *et al.*, "Elettra 2.0: the vacuum system design for a new generation storage ring", in *Proc. IPAC'23*, Venice, Italy, May 2023, pp. 4271-4274. doi:10.18429/JACoW-IPAC2023-THPA136

[5] T. Phimsen *et al.*, "Vacuum system of SPS-II: Challenges of conventional technology in Thailand new generation synchrotron light source", in *Proc. 12th Int. Conf. Mech. Eng. Design Synchrotron Radiat. Equip. Instrum. (MEDSI'23)*, Beijing, China, Nov. 2023, pp. 363-367. doi:10.18429/JACoW-MEDSI2023-FROAM02.

[6] A. Mathewson, "Vacuum System Design", presented at CERN Accelerator School: Vacuum Technology, Geneva, Switzerland, 1994, pp. 717–735.

[7] L. Palumbo, V. G. Vaccaro, and M. Zobov, "Wake Fields and Impedance", in *Proc. CAS – CERN Accelerator School: Advanced Accelerator Physic*s, Rhodes, Greece, Sep.–Oct. 1994, CERN-95-06, pp. 331–390. doi:10.5170/CERN-1995-006.331

[8] T. Rocha, "The Vacuum System of the Upcoming SIRIUS Light Source in Brazil", presented at Beam Dynamics Meets Vacuum, Collimations and Surfaces, Karlsruhe, Germany, Mar. 2017, unpublished.

[9] R. Parise *et al.*, "Prototyping for the ALBA II vacuum system", in *Proc. MEDSI'25*, Lund, Sweden, Sep. 2025, pp. 405-408. doi:10.18429/JACoW-MEDSI2025-THP58